



NURC

*a NATO Research Centre
un Centre de Recherche de l'OTAN*



Reprint Series

NURC-PR-2007-002

Multipath pulse shapes in shallow water: Theory and simulation

Chris Harrison, Peter L. Nielsen

April 2007

Originally published in:

Journal of the Acoustical Society of America, Vol. 121, No. 3, pp. 1362-1373,
March 2007

URL: <http://scitation.aip.org/dbt/dbt.jsp?KEY=JASMAN&Volume=121&Issue=3>

NURC, a NATO Research Centre

NURC conducts world class maritime research in support of NATO's operational and transformational requirements. Reporting to the Supreme Allied Commander Transformation, the Centre maintains extensive partnering to expand its research output, promote maritime innovation and foster more rapid implementation of research products.

The Scientific Programme of Work (SPOW) is the core of the Centre's activities and is organized into four Research Thrust Areas:

- Expeditionary Mine Countermeasures (MCM) and Port Protection (EMP)
- Reconnaissance, Surveillance and Undersea Networks (RSN)
- Expeditionary Operations Support (EOS)
- Command and Operational Support (COS)

NURC also provides services to other sponsors through the Supplementary Work Program (SWP). These activities are undertaken to accelerate implementation of new military capabilities for NATO and the Nations, to provide assistance to the Nations, and to ensure that the Centre's maritime capabilities are sustained in a fully productive and economic manner. Examples of supplementary work include ship chartering, military experimentation, collaborative work with or services to Nations and industry.

NURC's plans and operations are extensively and regularly reviewed by outside bodies including peer review of the research, independent national expert oversight, review of proposed deliverables by military user authorities, and independent business process certification. The Scientific Committee of National Representatives, membership of which is open to all NATO nations, provides scientific guidance to the Centre and the Supreme Allied Commander Transformation.



Copyright © Acoustical Society of America 2007

NOTE: The NURC Reprint series reprints papers and articles published by NURC authors in the open literature as an effort to widely disseminate NURC products. Users should cite the original article where possible.

Multipath pulse shapes in shallow water: Theory and simulation

Chris H. Harrison^{a)} and Peter L. Nielsen^{b)}

NATO Undersea Research Centre, Viale San Bartolomeo 400, 19126 La Spezia, Italy

(Received 27 September 2006; revised 19 December 2006; accepted 19 December 2006)

In shallow water propagation the steeper ray angles are weakened most by boundary losses. Regarding the sound intensity as a continuous function of angle it can be converted into a function of travel time to reveal the multipath pulse shape received from a remote source (one-way path) or a target (two-way path). The closed-form isovelocity pulse shape is extended here to the case of upward or downward refraction. The envelope of the earliest arrivals is roughly trapezoidal with a delayed peak corresponding to the slowest, near horizontal refracted paths. The tail of the pulse falls off exponentially (linearly in decibels) with a decay constant that depends only on the bottom reflection properties and water depth, irrespective of travel time, a useful property for geoacoustic inversion and for sonar design. The nontrivial analytical problem of inverting explicit functions of angle into explicit functions of time is solved by numerical interpolation. Thus exact solutions can be calculated numerically. Explicit closed-form approximations are given for one-way paths. Two-way paths are calculated by numerical convolution. Using the wave model C-SNAP in several broadband cases of interest it is demonstrated that these solutions correspond roughly to a depth average of multipath arrivals. © 2007 Acoustical Society of America. [DOI: 10.1121/1.2434691]

PACS number(s): 43.30.Gv, 43.30.Pc [RCG]

Pages: 1362–1373

I. INTRODUCTION

The multipaths of shallow water propagation spoil the resolution of active sonars by introducing a spread in travel times. The broadening of pulse transmission is therefore a nuisance to sonar detection and underwater communications (Urick, 1967; Atkinson, 1974; Sachs *et al.*, 1968). On the other hand it has been shown (Smith, 1971; Harrison, 2003a) that the pulse shape contains easily extractable environmental information. So for both reasons the shape of the pulse and its dependence on environmental properties are of interest. One could investigate these effects with ray traces, but here the more general behavior is established by studying the pulse shape analytically.

In a multipath shallow water environment acoustic travel times and boundary losses vary according to the trajectories of the rays. In the absence of additional constraints, such as source or receiver beam patterns, or target vertical directionality this results in a calculable spreading of the transmitted pulse shape. If the sonar system has a broad frequency band then individual eigenray arrivals may be seen inside this spread. If it has a narrow band then interference effects make the rays group into modal arrivals. In both cases the arrivals tend to increase their separation as time advances. The mathematical approach here is insensitive to these detailed arrivals because it treats the ray angles as a continuum. Nevertheless it takes account of both their changing amplitudes and their changing separations in such a way that the cumulative time integral of the pulse shape matches the more “steppy” cumulative integral of the true eigenray or mode arrival pulse shape. The pulse envelope calculated here corresponds physically to a depth average or locally range-averaged pulse

shape. The depth average is particularly close for the tail of the pulse where rays interact with both seabed and sea surface.

Smith (1971) and Harrison (2003a) investigated this behavior for isovelocity water and found that for a two-way path the received pulse decayed exponentially (i.e., the roll-off was a fixed number of decibels per unit time) with a time constant that was independent of travel time or range but fixed by the angle dependence of the reflection loss. Subsequently Prior and Harrison (2004) applied the findings to experimental data, and demonstrated that the derived reflection properties were consistent with the literature.

This paper extends the earlier analytical work on pulse shape first by including the critical angle’s truncation of the pulse (trivial for one-way path but not trivial for two-way path), and second by including a uniform vertical gradient refraction using the approach of Harrison (2003b). In both cases one-way and two-way paths are considered. The former would be appropriate for direct blast measurements while the latter would be appropriate for the multipath echo from a point target or an echo repeater. In this respect the approach contrasts with other active sonar inversion techniques based, for instance, on matched field processing of the one-way path (Siderius *et al.*, 2002), or inversion of reverberation (Preston *et al.*, 2005). This time spreading is still expected even if the target has a large horizontal extent which may lead to a “glint” near the horizontal specular direction. However, no such effect will be found if the target has a large vertical extent like, for example, the leg of an oil rig.

Finally some comparisons in three environments with the normal mode model C-SNAP demonstrate the relationship between the closed-form pulse shapes and the sequence of resolvable eigenray arrivals.

^{a)}Electronic mail: harrison@nurc.nato.int

^{b)}Electronic mail: nielsen@nurc.nato.int

II. EIGENRAYS

The approach in Harrison (2003a) was to calculate propagation intensity analytically as an eigenray sum in which there are so many eigenrays that their index can be treated as a continuum in angle. The intensity can be treated equivalently as a continuum of incoherent modes or as energy flux. The solution behaves like a local range average, retaining depth variation but eliminating rapid interference fluctuations and convergence effects. The technique has been applied to bistatic geometry (Harrison, 2005a), a refracting environment with flat seabed (Harrison, 2003b), and a refracting environment with sloping seabed (Harrison, 2005b). The power arriving at a remote receiver can be written as an integral over eigenray index, which can be converted, by change of variable, to an integral over angle (at the source or receiver). In the context of time smearing, for each eigenray the travel time and the angle are known, so the power can also be written as an integral in travel time. Since travel time can be resolved, the multipath pulse shape is the integrand in this time integral. So to find these functions in a refracting environment one can use the formulas already derived for propagation in terms of ray elevation angle θ or inverse cycle distance u in Harrison (2003b). A minor difficulty is in writing the result in terms of time t so that the pulse shape is an explicit function of time.

Generally, knowing a propagation formula as the integral of a quantity $Q(\nu)$ over a parameter ν , and knowing the conversion from ν to t one obtains a pulse shape $I_{1\text{way}}$,

$$I_{1\text{way}}dt = \left\{ Q(\nu(t)) \left| \frac{d\nu(t)}{dt} \right| \right\} dt \quad (1)$$

The modulus sign is required for the case where t is not a single-valued function of ν , for instance ν could be angle. Integrating $I_{1\text{way}}$ in t would, of course, give the same result as integrating $Q(\nu)$ in ν . Both can be interpreted as either the linear form of transmission loss ($10^{-TL/10}$) or the energy per unit area resulting from a unit energy source. Thus $I_{1\text{way}}$ would be an intensity. The isovelocity case will be recapitulated in Sec. III. The pulse shape for the two-way path is given by the convolution of the one-way pulse shape $I_{1\text{way}}$ with itself,

$$I_{2\text{way}}dT = \int_0^T I_{1\text{way}}(t)I_{1\text{way}}(T-t)dt dT. \quad (2)$$

The function $I_{1\text{way}}$ may be discontinuous or split into several regions in each of which there is one continuous function. For a one-way path this is straightforward, but for the two-way path the convolution will contain several cross-term contributions with various integration limits.

III. REVIEW OF PULSE SHAPE WITH ISOVELOCITY WATER

A. One-way path

Following Harrison (2003a) the total time for a ray, tilted at θ , to travel a horizontal distance r at speed c is given by

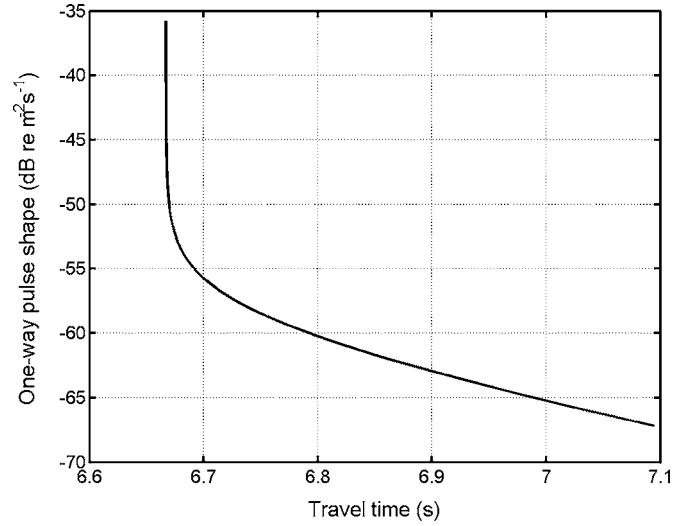


FIG. 1. One-way pulse shape in isovelocity water.

$$t = (r/c)\sec \theta \cong (r/c) + (r/2c)\theta^2. \quad (3)$$

In terms of the delay after first arrival τ this is

$$\tau = t - r/c = r\theta^2/2c, \quad (4)$$

$$d\tau = (r/c)\theta d\theta. \quad (5)$$

The received energy for a unit energy source is

$$E = \frac{2}{rH} \int_0^{\theta_c} \exp\left\{-\frac{\alpha\theta^2 r}{2H}\right\} d\theta, \quad (6)$$

where H , θ , θ_c are water depth, horizontal angle, and critical angle, and $\alpha\theta$ is a linear approximation to $\log(R)$, i.e., bottom reflection loss in dB is $RL = 20 \log_{10}(R) = \alpha_{\text{dB}}\theta$, where $\alpha = \alpha_{\text{dB}}/(10 \log_{10} e)$. This converts to a one-way pulse shape

$$I_{1\text{way}}d\tau = \frac{2}{rH} \frac{\exp\{-\alpha\tau/t_H\}}{\sqrt{2t_0\tau}} d\tau, \quad (7)$$

where $t_0 \equiv r/c$ is the delay time to the first arrival and $t_H = H/c$.

To the earlier derivation is added the condition that this equation is valid for $0 < \tau < \tau_c$ where τ_c corresponds to the critical angle θ_c . Elsewhere $I_{1\text{way}} = 0$. The behavior of this function is shown in Fig. 1. In this example $r = 10$ km, $\alpha_{\text{dB}} = 1$ dB, $\theta_c = 20^\circ$, $H = 100$ m. Units will be discussed in detail in Sec. VI. For now note that the mathematical quantity $I_{1\text{way}}$ in Eq. (7) has explicit dimensions of per unit area per unit time. Thus the y axis is labeled dB re $\text{m}^{-2} \text{s}^{-1}$. Notice that in the angle or travel time continuum case the first arrival is a singularity. This is because in the continuum the interval between eigenray arrivals goes to zero at this point. In reality, of course, eigenrays are discrete so the interval between first and second arrival is finite. Nevertheless the total energy in the pulse (integral $d\tau$) is finite since it has just been transformed from the, more obviously finite, integral in θ .

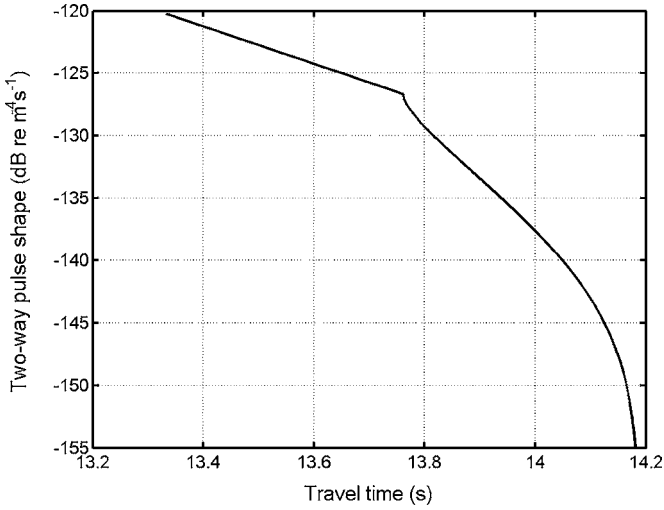


FIG. 2. Two-way pulse shape in isovelocity water. The early part is exponential (linear in dB).

B. Two-way path

The derivation in Harrison (2003a) for a two-way path T is correct in the absence of a critical angle, and is in any case correct for $T < \tau_c$. Otherwise the critical angle's truncation of the one-way pulse introduces a second functional form between delays τ_c and $2\tau_c$, beyond which $I_{2\text{way}}$ is zero. The integral has the same form as Eq. (53) in Harrison (2003a) but with different limits. Thus for $0 < T \leq \tau_c$ it is

$$\begin{aligned}
 I_{2\text{way}} dT &= \frac{2}{r^2 H^2 t_0} \int_0^T \frac{1}{\sqrt{\tau_1(T - \tau_1)}} d\tau_1 \exp\{-\alpha T/t_H\} dT \\
 &= \frac{2}{r^2 H^2 t_0} \int_{\tau'=-T/2}^{\tau'=T/2} \frac{1}{\sqrt{(T/2)^2 - \tau'^2}} d\tau' \\
 &\quad \times \exp\{-\alpha T/t_H\} dT \\
 &= \frac{2}{r^2 H^2 t_0} [\text{asin}(2\tau'/T)]_{-T/2}^{T/2} \exp\{-\alpha T/t_H\} dT \\
 &= \frac{2\pi}{r^2 H^2 t_0} \exp\{-\alpha T/t_H\} dT. \tag{8}
 \end{aligned}$$

For $\tau_c < T < 2\tau_c$ it is

$$\begin{aligned}
 I_{2\text{way}} dT &= \frac{2}{r^2 H^2 t_0} \int_{\tau'=(\tau_c - T/2)}^{\tau'=\tau_c - T/2} \frac{1}{\sqrt{(T/2)^2 - \tau'^2}} d\tau' \\
 &\quad \times \exp\{-\alpha T/t_H\} dT \\
 &= \frac{4}{r^2 H^2 t_0} \text{asin}((2\tau_c/T) - 1) \exp\{-\alpha T/t_H\} dT. \tag{9}
 \end{aligned}$$

The behavior of the complete function is shown in Fig. 2. Parameters are the same as in Fig. 1. There is no singularity as was seen with the one-way path, and the angle discontinuity separating the two functions is clearly visible in the middle. Note that this quantity is the time domain representation of two-way propagation loss with one grand smearing. Its units are therefore per unit area-squared per unit time.

IV. PULSE SHAPE WITH REFRACTION

To calculate dv/dt in Eq. (1) one needs formulas for travel time and cycle distance. In an environment with a uniform sound speed gradient c' between upper and lower sound speed values c_H, c_L (c_H may be physically at the top or the bottom of the water column) the cycle distance for a ray with a turning point velocity c_T is

$$d_0 = \frac{2}{|c'|} (|\sqrt{c_T^2 - c_L^2} - \sqrt{c_T^2 - c_H^2}|) \tag{10}$$

and the cycle travel time can be expressed in three ways:

$$\begin{aligned}
 \tau_0 &= \frac{1}{|c'|} \left(\left| \ln\left(\frac{1 + \sin \theta_L}{1 - \sin \theta_L}\right) - \ln\left(\frac{1 + \sin \theta_H}{1 - \sin \theta_H}\right) \right| \right) \\
 &= \frac{2}{|c'|} (|\text{atanh}(\sin \theta_L) - \text{atanh}(\sin \theta_H)|) \\
 &= \frac{2}{|c'|} (|\text{asinh}(\tan \theta_L) - \text{asinh}(\tan \theta_H)|). \tag{11}
 \end{aligned}$$

Throughout this paper subscripts L and H are attached to various properties to denote their values at the boundary corresponding to low sound speeds (L) or high sound speeds (H). The total one-way travel time can be written in terms of the horizontal cycle distance and the cycle travel time

$$t = \frac{r\tau_0}{d_0}. \tag{12}$$

This can easily be generalized to a piece-wise linear depth dependence (Harrison, 2006), and this method will be used in the last test case of Sec. VI.

Harrison (2003b) gives explicit formulas for propagation intensity with a flat seabed and uniform sound speed gradient. At very high frequencies one expects to find the effects of caustics, manifest in the depth dependence, but at lower frequencies they are expected to be less important. Propagation and reverberation intensities are calculated with, and without, caustic effects; in the main derivations here caustics are ignored although they are reconsidered in the context of the test cases in Sec. VI. Justification for this at frequencies of a few kilohertz or below is given in Appendix A of Harrison (2005b).

Note that the exact formulas from Harrison (2003b) for $\tan \theta_L$ and $\tan \theta_H$ are consistent with the exact formula for cycle distance [Eq. (10)] and cycle travel time [Eq. (11)]. Although, in the isovelocity case, a small angle approximation was introduced, all efforts are made, in the refraction case, to avoid approximations in calculating times (as opposed to intensities) until absolutely necessary because of the more complicated behavior.

There are two refraction regimes: In the first, rays have one refraction turning point and interact with only one boundary (the low speed side); in the second, rays interact with both boundaries.

A. One-way path: Single boundary interaction

Following Sec. 2.2.1 of Harrison (2003b) when rays interact with only one boundary the cycle distance d_0 and its reciprocal u are given exactly by

$$d_0 = u^{-1} = (2c_L/c') \tan \theta_L. \quad (13)$$

To avoid making *ad hoc* approximations at this stage, the mathematically convenient relationship $R = \alpha \tan \theta$ for each reflection is assumed at the outset. Therefore the total boundary loss at a fixed range r is independent of angle (and therefore time)

$$\alpha_L \tan \theta_L r u = \alpha_L \tan \theta_L r c' / (2c_L \tan \theta_L) = \alpha_L r c' / (2c_L). \quad (14)$$

The original equation [Eq. (2.6), Harrison, 2003b] was written as an integral in the parameter u . From Eq. (12) the total travel time t can also be written in terms of u ,

$$\begin{aligned} t &= \frac{r\tau_0}{d_0} = ur\tau_0 = \frac{2ru}{c'} \operatorname{asinh}(\tan \theta_L) = \frac{r \operatorname{asinh}(\tan \theta_L)}{c_L \tan \theta_L} \\ &= \frac{2ru}{c'} \operatorname{asinh}\left(\frac{c'}{2c_L u}\right). \end{aligned} \quad (15)$$

Since the exact maximum and minimum values of u are, respectively,

$$u_{\max} = \sqrt{c'/(4h_{\text{sr}}(c_{\text{sr}} + c_L))}, \quad (16)$$

$$u_{\min} = \sqrt{c'/(4H(c_H + c_L))}, \quad (17)$$

where H , c_L , c_H are water depth and sound speeds at the boundaries (high and low). The gradient is $c' = (c_H - c_L)/H$. The greater of the sound speeds at the source and receiver is c_{sr} , and the corresponding distance of this point from the low speed boundary is h_{sr} . Thus h_{sr} is a depth in an upward refracting environment but a height from the seabed in a downward refracting environment.

The corresponding exact minimum and maximum values of $\tan \theta_L$ are

$$\tan \theta_{L\min} = \sqrt{(c_{\text{sr}}/c_L)^2 - 1}, \quad (18)$$

$$\tan \theta_{L\max} = \sqrt{(c_H/c_L)^2 - 1}. \quad (19)$$

Substitution into Eq. (15) gives exact maximum and minimum travel times,

$$t_{\max} = r \operatorname{asinh}\left(\sqrt{(c_{\text{sr}}/c_L)^2 - 1}\right) / \sqrt{(c_{\text{sr}}^2 - c_L^2)}, \quad (20)$$

$$t_{\min} = r \operatorname{asinh}\left(\sqrt{(c_H/c_L)^2 - 1}\right) / \sqrt{(c_H^2 - c_L^2)}. \quad (21)$$

A straightforward numerical approach to evaluating Eq. (1) is first to differentiate Eq. (15) with respect to u to obtain du/dt as a function of u ,

$$\frac{du}{dt} = u/(t - (r/c_L) \operatorname{sech}(tc'/(2ru))), \quad (22)$$

then the function $t(u)$ [in Eq. (15)] can be inverted to $u(t)$ by simply interpolating it on to a linear grid of t .

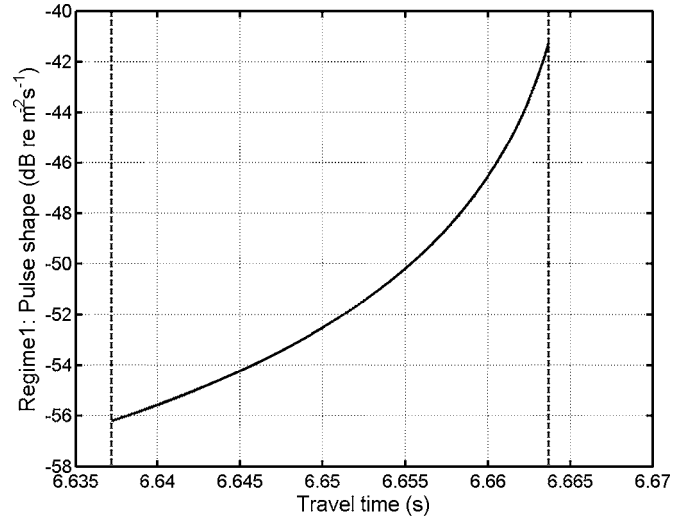


FIG. 3. Contribution to the pulse for refraction regime 1, bounded by the times t_{\min} and t_{\max} . Parameters are $c_L = 1500$ m/s, $c_H = 1520$ m/s, $r = 10$ km, $\alpha_{L\text{dB}} = 1$ dB, $\alpha_{H\text{dB}} = 0$ dB, $H = 100$ m, and $z_{\text{sr}} = 90$ m.

Following Eq. (1) and adopting Eq. (22) leads to a formula for the single boundary interaction part (regime 1) of the pulse shape

$$\begin{aligned} I_1 dt &= \frac{4}{r} \exp(-R_L r u) \frac{du}{dt} dt \\ &= \frac{4}{r} u / (t - (r/c_L) \operatorname{sech}(tc'/(2ru))) dt \exp\{-\alpha_L c' r / (2c_L)\} \end{aligned} \quad (23)$$

whose functional form in t can be seen by interpolation using Eq. (15).

In most of this paper it is assumed that bottom loss is linear with tangent of angle, however, the interpolation approach allows one to drop this assumption and take an arbitrary curve, as implied by the first line of Eq. (23) (R_L is the natural logarithm of the power reflection coefficient of the L boundary, i.e., on the low sound speed side). This will be useful in later comparisons with a wave model. An example with parameters $c_L = 1500$ m/s, $c_H = 1520$ m/s, $r = 10$ km, $\alpha_{L\text{dB}} = 1$ dB, $\alpha_{H\text{dB}} = 0$ dB, $H = 100$ m, $z_{\text{sr}} = 90$ m is shown in Fig. 3 (z_{sr} is the complement of h_{sr} , i.e., $z_{\text{sr}} = H - h_{\text{sr}}$). The vertical dotted lines denote t_{\min} and t_{\max} .

To find an explicit functional form in t one needs to make an approximation. There are various approaches which are elaborated in Appendix A. The resulting approximate contribution to the pulse shape can be written as an explicit function of t (and $t_L = r/c_L$),

$$I_1 dt = \frac{dt}{(t_L - t)^{3/2}} \left\{ \frac{t_L^{3/2} c'}{\sqrt{6} r^2} \exp[-(\alpha_L c' / (2c_L)) r] \right\}. \quad (24)$$

The factor in curly braces does not affect the pulse shape of this contribution but it does control the amplitude relative to the two-boundary contribution. It is clear from the form of Eq. (24) that a singularity is possible when $t = t_L$. Usually this is precluded by the fact that $t_{\max} < t_L$, however, if both the source and receiver are on the “ L ” boundary then $t_{\max} = t_L$ [see Eq. (20)]. One could superimpose a plot of Eq. (24)

on the exact curve in Fig. 3 [i.e., Eq. (23)], however visual discrimination would be difficult since the mean difference is 0.1% in this case. This figure becomes 0.5% with $z_{sr}=10$ m, and reduces with sound speed contrast.

B. One-way path: Two-boundary interaction

Following Sec. 2.2.2 of Harrison (2003b) the total boundary loss is $(\alpha_L \tan \theta_L + \alpha_H \tan \theta_H)ru$, and the relationship between angles at the low and high speed boundaries θ_L , θ_H and cycle distance d_0 and its reciprocal u are given exactly by

$$\tan \theta_L = 2Hua_L + c'/(4c_L u), \quad a_L = 1 + Hc'/2c_L, \quad (25)$$

$$\tan \theta_H = 2Hua_H - c'/(4c_H u), \quad a_H = 1 - Hc'/2c_H, \quad (26)$$

$$t = \frac{2ru}{c'} (\operatorname{asinh}\{2Hua_L + c'/(4c_L u)\} - \operatorname{asinh}\{2Hua_H - c'/(4c_H u)\}). \quad (27)$$

The limits on u , θ , and t are as follows taking θ_c to be the smaller critical angle of the two boundaries. Strictly the upper limit on u is given by Eq. (25) with $\theta_L = \theta_c$, but it is approximately

$$u_{\max} \cong \tan \theta_c / 2H, \quad (28)$$

$$u_{\min} = \sqrt{c'/(4H(c_H + c_L))}. \quad (29)$$

Note that this second limit is the same as for regime 1 and that insertion into Eq. (27) leads to the same formula for t since the second term vanishes. The corresponding exact minimum and maximum values of $\tan \theta_L$ are

$$\tan \theta_{L\max} = \tan \theta_c, \quad (30)$$

$$\tan \theta_{L\min} = \sqrt{(c_H/c_L)^2 - 1}. \quad (31)$$

Substitution into Eq. (15) gives exact maximum and minimum travel times

$$t_{\max} = (r/c_L) \operatorname{asinh}(\tan \theta_c) / \tan \theta_c, \quad (32)$$

$$t_{\min} = r \operatorname{asinh}(\sqrt{(c_H/c_L)^2 - 1}) / \sqrt{(c_H^2 - c_L^2)}. \quad (33)$$

Again, a numerical solution is straightforward. Differentiating Eq. (27) with respect to u leads, after some manipulation, to

$$\frac{du}{dt} = u \left/ \left\{ t - \frac{2r}{\sqrt{\{2Hu(c_H + c_L)\}^2 + (c'/2u)^2 + 2(c_L^2 + c_H^2)}} \right\} \right. \quad (34)$$

From Eq. (2.17) Harrison (2003b) the pulse shape for the two-boundary-interacting component is

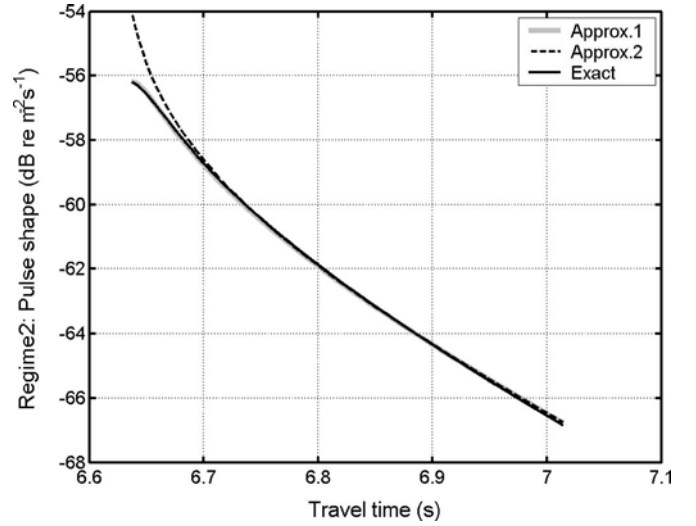


FIG. 4. Contribution to the pulse for refraction regime 2: “Exact” (solid black line); “Approx.1” [Eq. (36)] (thick grey line, partially obscured); “Approx.2” [Eq. (37)] (black dashed line). Parameters are $c_L=1500$ m/s, $c_H=1520$ m/s, $r=10$ km, $\alpha_{LdB}=1$ dB, $\alpha_{HdB}=0$ dB, $H=100$ m, and $z_{sr}=90$ m.

$$\begin{aligned} I_2 dt &= \frac{4}{r} \exp\{-(R_L + R_H)ru\} \frac{du}{dt} \\ &= \frac{4}{r} \exp\{-(\alpha_L \tan \theta_L + \alpha_H \tan \theta_H)ru\} \frac{du}{dt} \\ &= \exp\{-2rHu^2(\alpha_L a_L + \alpha_H a_H)\} \frac{du}{dt} \\ &\quad \times \left\{ \frac{4}{r} \exp\{-c'r(\alpha_L/c_L - \alpha_H/c_H)/4\} \right\} \quad (35) \end{aligned}$$

with a_L and a_H given by Eqs. (25) and (26). By using Eq. (27) to interpolate to t and Eq. (34) for du/dt the exact result is plotted in Fig. 4 with the same parameters as for regime 1 in Fig. 3. It is already clear that this solution must be close to that for the isovelocity case [Eq. (7)] for large τ . The first line of Eq. (35) is a reminder that the interpolation approach allows one to adopt arbitrary boundary loss R_L , R_H and to drop the assumption of linearity.

To find a pulse shape that is an explicit function of t one needs to make an approximation to Eqs. (27) and (28), but there are many choices, and there are two aims. First one seeks a compromise between accuracy and simplicity, and second, one seeks a solution that is simple enough in form to convolve with itself and with the regime 1 contribution [Eq. (24)] in order to derive a two-way pulse shape. The former succeeds but unfortunately the latter does not. Two contenders are derived in Appendix A using, respectively, Eq. (A16) and Eq. (A17) but both using Eq. (A14), and these are compared with the exact solution in Fig. 4. As functions of t these two approximations are, respectively,

$$\begin{aligned} I_2 dt &= \left(\frac{t}{\sqrt{b_1 t + b_0}} - \frac{1}{\sqrt{c_2 t^2 + c_1 t + c_0}} \right)^{-1} \\ &\quad \times \exp(-a_1 t - a_0) dt 2Hf_0, \quad (36) \end{aligned}$$

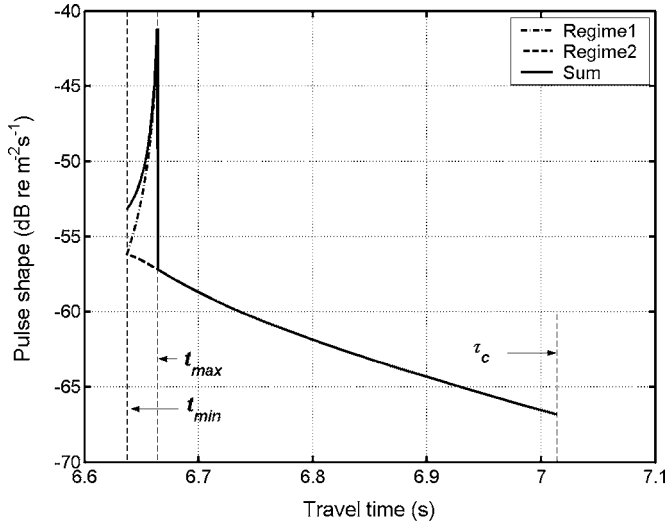


FIG. 5. Contributions to the pulse shape from refraction regime 1 (dash-dot line), regime 2 (dashed line), and their sum during the period in which they overlap (solid line). Parameters are as in Figs. 3 and 4.

$$I_2 dt = \frac{t}{\sqrt{t^2 - t_0^2}} \exp(-a_1 t - a_0) \frac{1}{t_0} dt f_0, \quad (37)$$

where the constants a_0 , a_1 , b_0 , b_1 , c_0 , c_1 , c_2 , f_0 , t_0 are given in Appendix A.

Note that the decay rate a_1 reduces to $(\alpha_L a_L + \alpha_H a_H)/t_H$ through Eq. (A13) if t_H is redefined as travel time across the water depth with an average sound speed. It is therefore still independent of travel time or range as in the isovelocity case. Comparing these formulas with the isovelocity case, Eq. (7), one finds that both equations converge on it as $c_L \rightarrow c_H$.

C. Two-way path: Numerical convolution

The pulse shapes for the two regimes overlap in time (see Figs. 3 and 4), but since the rays are considered to be incoherent their powers can be added to obtain an overall pulse shape as shown in Fig. 5. The characteristic trapezoidal or sail shape consists of a rise from first arrival at $t=t_{\min}$ with a later peak at $t=t_{\max}$ (rarely a singularity), followed by a sudden drop to an exponential decay which continues until $t=t_c$ at the critical angle. Thus between t_{\min} and t_{\max} the pulse shape is one explicit, continuous function, and between t_{\max} and t_c it is another. From the point of view of convolving the pulse by itself as in Eq. (2) there are three integrals to be formed, each with various limits. Here it has been tacitly assumed that the two-way paths go from source to receiver and back to source location. Clearly many permutations are possible if the source and receiver are separated. The calculation then consists of the convolution of the two different one-way pulse shapes. So far, the search for approximations to these functions that can be integrated analytically has been unsuccessful, so a simpler approach is numerical convolution. Three examples of pulse shapes for two-way paths are shown in Fig. 6 for the same parameters as in Fig. 5 but with $z_{sr}=90, 50,$ and 10 m. The dashed lines show the isovelocity equivalent based on the average sound speed for comparison. More examples are given in Harrison (2006).

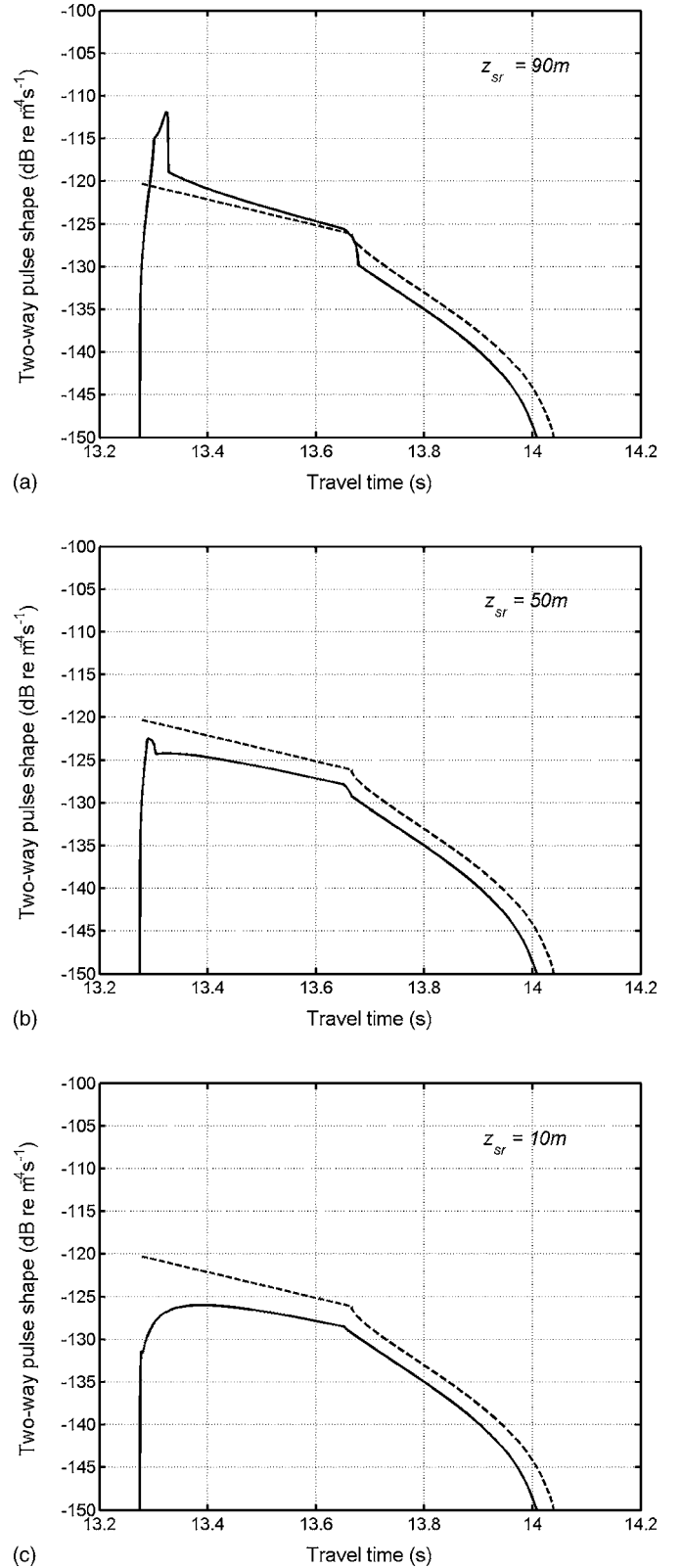


FIG. 6. Two-way pulse shape (solid) for parameters as in Fig. 5 except that z_{sr} (depth of the shallowest of source and receiver) takes values: (a) 90 m, (b) 50 m, and (c) 10 m. Isovelocity equivalent for average sound speed superimposed (dashed line).

V. RULES OF THUMB

It is possible to describe the one-way trapezoid shape roughly through two parameters. These are the time spread

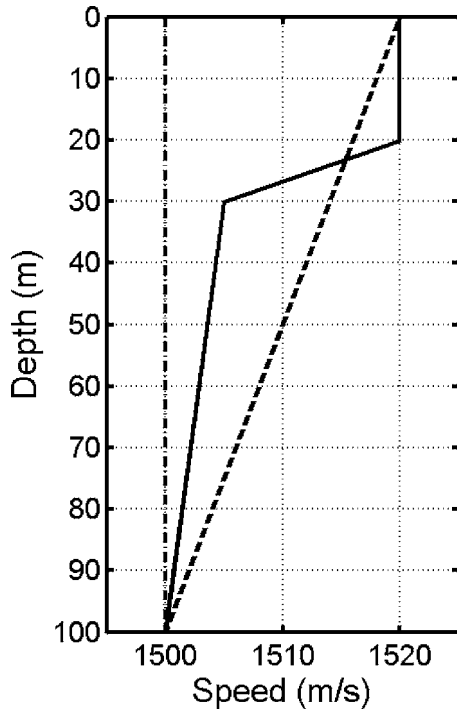


FIG. 7. Sound speed profiles for test cases: Case 1, isovelocity (dash-dot line), case 2, uniform gradient (dashed line), and case 3, “summer” (solid line).

of the regime 1 contribution, T_0 (i.e., the time difference between the first arrival and the peak $T_0 = t_{\max} - t_{\min}$), and the ratio of intensities at these two times F_0 . The right-hand sides of Eqs. (20) and (21) are both of the form $r/c_L \times \text{asinh}(X)/X$, so their difference can be written in terms of the series expansion as

$$\frac{\text{asinh}(X)}{X} - \frac{\text{asinh}(Y)}{Y} = -\frac{X^2 - Y^2}{3!} + \dots \quad (38)$$

So the time difference can be written in terms of the range, sound speed gradient, and $z_{\text{sr}} (z_{\text{sr}} = H - h_{\text{sr}})$, or in terms of sound speed contrast $\delta c_{\text{sr}} = c_H - c_{\text{sr}}$ and travel time $t_L = r/c_L$ as

$$T_0 = t_{\max} - t_{\min} = \frac{r}{6c_L^3} (c_H^2 - c_{\text{sr}}^2) \approx \frac{r z_{\text{sr}} c'}{3c_L^2} \approx \frac{1}{3} t_L \frac{\delta c_{\text{sr}}}{c_L}. \quad (39)$$

As one might expect, putting either source or receiver near the high speed boundary (small z_{sr}) or weakening the sound speed gradient results in a smaller angle range for regime 1 and therefore a shorter time spread.

According to Eq. (24) the ratio of intensities at these two times is

$$F_0 = \left(\frac{t_L - t_{\min}}{t_L - t_{\max}} \right)^{3/2}. \quad (40)$$

Again invoking Eqs. (20) and (21) and expanding their series to first order one finds

$$F_0 = \left(\frac{c_H^2 - c_L^2}{c_{\text{sr}}^2 - c_L^2} \right)^{3/2} = \left(\frac{H(c_H + c_L)}{(H - z_{\text{sr}})(c_{\text{sr}} + c_L)} \right)^{3/2} \approx \left(\frac{H}{(H - z_{\text{sr}})} \right)^{3/2} = \left(\frac{H}{h_{\text{sr}}} \right)^{3/2}. \quad (41)$$

To a good approximation the intensity ratio just depends on the proximity of the (closest of) source and receiver to the high speed boundary. In summary it is possible to control the pulse shape to a certain extent: The sail shape is most pronounced if both source and receiver are close to the low speed boundary; it is least pronounced and the pulse resembles the isovelocity case when one or both are near the high speed boundary. The tail of the pulse, with or without refraction, has an exponential decay that depends on reflection loss and water depth only. The shape of the tail is therefore independent of range.

As mentioned at the beginning of Sec. IV C it has been assumed that two-way paths are from source to receiver and back to the same source location. Of course, in reality there are multipaths between source and target and then between target and receiver, all of which may be at different depths. The above-mentioned rules of thumb are for one-way paths, and one can still combine their results assuming different end point depths on the outward and return paths.

VI. COMPARISON WITH A WAVE MODEL

Section I alluded to the fact that the approach used here is based on a continuum of rays or modes whereas in reality one may be able to discriminate actual rays with a broad band system or actual modal arrivals with a narrow band system. To make this comparison more concrete and to check the results the wave model C-SNAP (Ferla *et al.*, 1993) is run and averages devised to demonstrate the agreement explicitly. In the following, three test cases are considered: isovelocity, uniform downward refraction, and a three layer summer profile with a thermocline.

For the given range and source and receiver depths C-SNAP calculates a normal mode solution at 2000 frequencies between 500 and 1500 Hz. This is then shaded and Fourier transformed to form a received time series. To ensure correspondence with the analytical solutions the time series is normalized by also forming a source time series and calculating its integral of pressure squared over time. Thus there is effectively a unit energy source resulting in a received intensity, and the units of the response are intensity per unit source energy or $\text{m}^{-2} \text{s}^{-1}$, as already noted for the closed-form solutions (see also Hall, 1995; Ainslie and Beerens, 2005).

A further step needs to be taken because the time series resolves eigenrays, given a wide frequency band (or resolves modal arrivals for a narrow band). In principle these can be smoothed out with an average in travel time or range or depth. It is inevitable that in the tail of the smoothed pulse, where rays interact with both boundaries, the eigenray delays vary uniformly and continuously with depth so a depth average is appropriate. In the early part of the pulse for the refraction cases the analytical solution is also a function of depth so one can also compare the depth average of the ana-

TABLE I. Seabed and water half-space parameters.

	Sound speed c (m/s)	Density d (kg/m ³)/1000	Vol. absorption a (dB/wavelength)
Water	1500	1.0	0.0
Sediment	1580	1.5	0.1

lytical solution with the depth average of the normal mode solution. The formulas in the main text ignore focusing and caustic effects, however, following Weston (1980) it is straightforward to include them, as well as depth averaging, as explained in Appendix B.

All cases assume a water depth of 100 m, a source depth of 50 m, and a range of 50 km. Sound speed profiles are shown in Fig. 7, and the seabed is assumed to be a half-space, although this is not a restriction, with parameters given in Table I. The relevant part of the Rayleigh reflection coefficient is shown in Fig. 8. Notice that the linear approximation to reflection loss is very good up to about 16° (the critical angle is 18.3° , α is 0.32 rad^{-1} , and $\alpha_{\text{dB}} = 1.39 \text{ dB/rad}$). At worst it overestimates the loss by about 0.04 dB near 12° .

A. Isovelocity case

Figure 9 shows the closed-form solutions superimposed on the depth average of the C-SNAP isovelocity solution. The dashed line is the linear reflection loss approximation using Eq. (7) or (35), and the solid line is for Rayleigh reflection loss using the top line of Eq. (35). Considering the large number of eigenrays, and therefore bottom reflections (~ 80 near the critical angle), the Rayleigh curve is an extremely good fit. The slight misfit of the linear curve at around 34 s is entirely due to the small discrepancy seen in Fig. 8 of about +0.04 dB in 0.25 dB. The value of α quoted for the curve in Fig. 8 is based on the Rayleigh gradient at

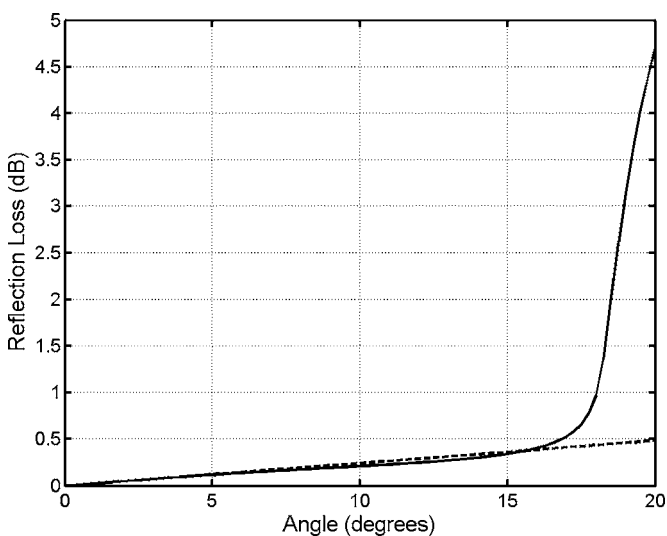


FIG. 8. Relevant part of the power Rayleigh reflection coefficient for half-space parameters as in Table I (solid line), and the linear approximation to it (dashed line). The difference reaches 0.04 dB at about 12° . The value of α is 0.32 ($\alpha_{\text{dB}} = 1.39$).

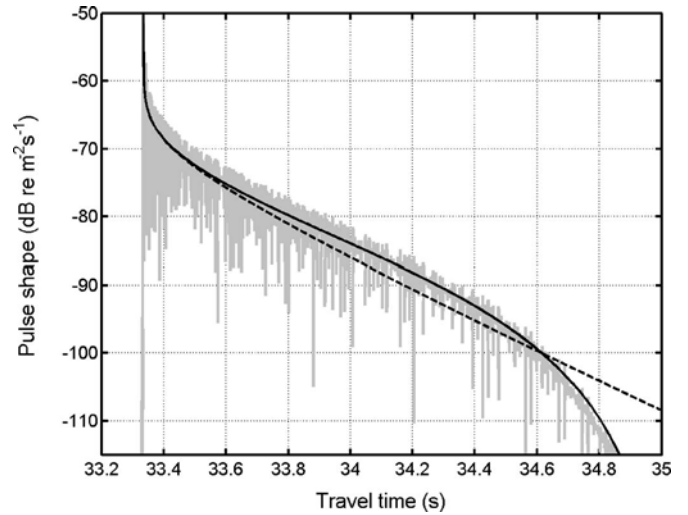


FIG. 9. Depth averaged pulse shape computed by C-SNAP for isovelocity water overlaying a half-space seabed defined by parameters in Table I (grey). Superimposed are the analytical solutions with Rayleigh reflection coefficient (black solid line), and linear approximation (dashed line).

the origin. In spite of this, an experimental measure of the fall-off rate of the pulse would lead to a reasonably accurate estimate of this slope.

B. Uniform gradient

The depth-averaged uniform gradient C-SNAP curve is shown as grey in Fig. 10, and one can see a pronounced refraction peak (regime 1). Superimposed are two curves, both using the Rayleigh reflection loss as in the first lines of Eqs. (23) and (35). To compare like with like the closed-form formulas are depth averaged as described in Appendix B. The solid line excludes caustic effects (a low frequency approximation), and the dashed line includes them (a high fre-

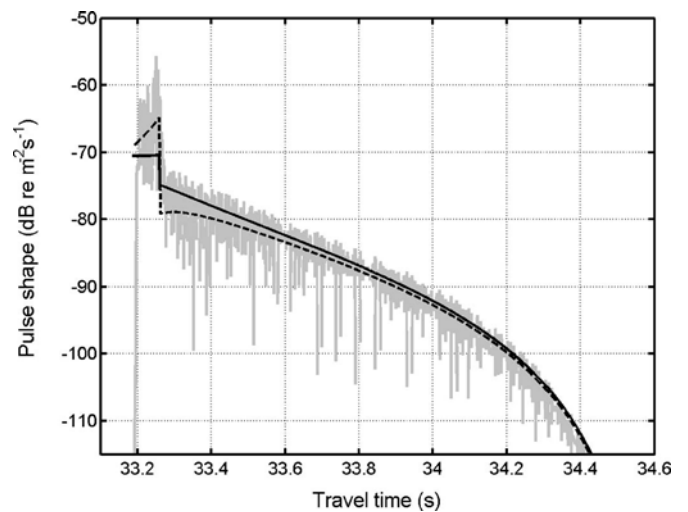


FIG. 10. Depth averaged pulse shape computed by C-SNAP for uniform sound speed gradient overlaying a half-space seabed defined by parameters in Table I (grey). Superimposed are the analytical solutions (also depth averaged) with Rayleigh reflection coefficient, excluding (black solid line), and including focusing effects (dashed line).

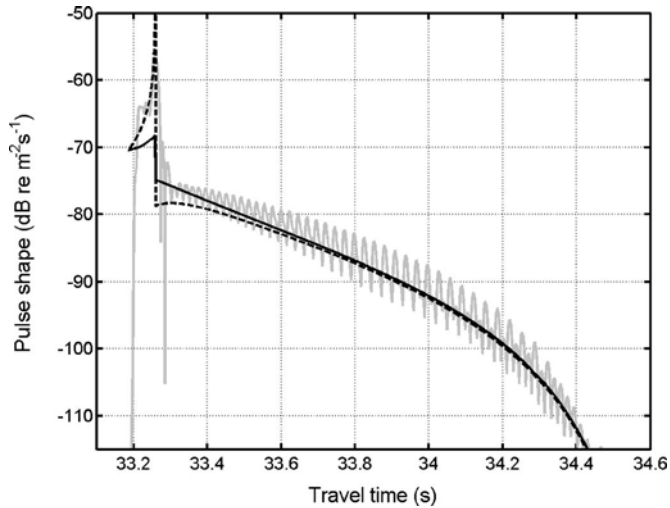


FIG. 11. Temporally smoothed pulse shape computed by C-SNAP for uniform sound speed gradient overlying a half-space seabed defined by parameters in Table I (grey line). Source and receiver depths are both 50 m. Superimposed are the analytical solutions with Rayleigh reflection coefficient, excluding (black solid line), and including focusing effects (dashed line).

quency approximation), making the modifications described in Appendix B. Both curves are very close to C-SNAP and more or less span its spread.

A more ambitious comparison is to exclude the depth averaging in all three cases and fix the source and receiver both at 50 m depth where there is a caustic (Brekhovskikh and Lysanov, 1982). The caustic occurs when the ray angle at the source is horizontal which corresponds to the latest refracting (regime 1) arrival, or the peak in Fig. 11. The C-SNAP result is smoothed in time in order not to interfere with its depth variations. Again closed-form solutions are superimposed including and excluding caustics. Agreement is particularly good when caustics are included, bearing in mind that the mean of the C-SNAP curve is 2 or 3 dB below its peak values.

C. Arbitrary summer profile

Using Eqs. (10) and (11) piece-wise one can construct the components of Eq. (1), and therefore a pulse shape, numerically. This has been done with, and without, caustics, for the summer profile from Fig. 7, and superimposed on the C-SNAP solution in Fig. 12. Before considering the details of the early arrivals it is worth noting that in all cases so far there is a clear point in time beyond which the pulse shape is linear in decibels, or at least a direct mapping of the reflection coefficient. This is important from the point of view of inversion. This delay time is determined by the slowest refracting path (i.e., that which does not reflect from both boundaries). In the uniform gradient case this time is given by t_{\max} [Eq. (20)], which in that case is 33.26 s, as seen in the plots. In the summer profile case the slowest ray is no longer the horizontal ray at the source. Instead it is the one whose turning point is at the top of the thermocline (20 m), since the strong curvature steepens the rays in the relatively slow bottom layer. Rays that remain in the bottom layer must arrive, according to Eqs. (20) and (21), between 33.296 and

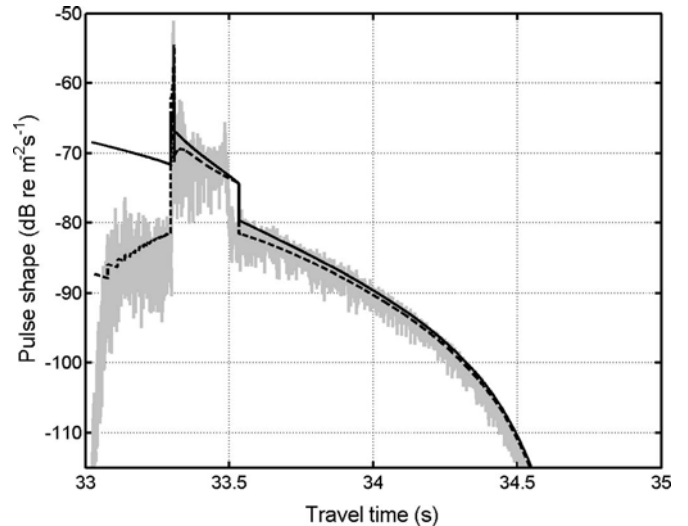


FIG. 12. Depth averaged pulse shape computed by C-SNAP for a summer sound speed profile overlying a half-space seabed defined by parameters in Table I (grey). Superimposed are the analytical solutions (also depth averaged) with Rayleigh reflection coefficient, excluding (black solid line), and including focusing effects (dashed line).

33.307 s, and are seen as the spike in the figure. Earlier delays than this correspond to rays that are just steep enough to enter the top fast layer. Because a very narrow range of angles at the source accounts for a large range of very long cycle distances the neglect of focusing effects becomes important. This explains the misfit of the solid line from 33.0 to 33.3 s but the relatively good fit of the dashed line. Otherwise the fit of both lines is extremely good for delays beyond about 33.3 s.

VII. CONCLUSIONS

This paper has derived formulas for the envelope of a multipath pulse in a shallow water environment with a uniform sound speed gradient. Variants are included for more general profiles. The refracted arrivals that interact only with the low sound speed boundary form a characteristic quadrilateral, or sail shape, near the leading edge of the pulse. In contrast, the steeper rays that interact with both boundaries form a long tail that decays more or less exponentially (linearly in decibels) with a rate dependent only on the reflection loss and the water depth. Furthermore this rate is independent of range or refraction. Some rules of thumb enable one to estimate the duration of the first refracted arrival [Eq. (39)] and the intensity ratio of its maximum and minimum [Eq. (41)].

Two approaches were taken to calculate the complete pulse shape. One was to write an exact expression [Eqs. (23) and (35)] in terms of mixed variables (time, cycle distance, and derivatives) which require interpolation to reveal pulse shape. The other was to make approximations to find explicit functions of time [Eqs. (24), (36), and (37)]. Two-way pulse shapes were obtained by numerical convolution rather than attempting analytical convolution, as was possible in the isovelocity case.

To establish correspondence between these pulse shapes and the expected eigenray or modal arrivals, three compari-

sons were made against the normal mode model C-SNAP, transforming its output into the time domain. The formulas for the three cases, isovelocity, uniform sound speed gradient, and summer profile, show very good agreement with a depth average or a time smoothing. Also the interpolation approach can easily handle the Rayleigh reflection loss, instead of its linear approximation.

The reasons for interest in the multipath pulse shape are threefold. First, the pulse shape is a useful predictor of geoaoustic properties because the tail of the pulse (i.e., the part later than the slowest refracting arrival) decays at a rate that depends only on water depth and angle derivative of reflection loss. In addition it is readily available for any existing active sonar. Equation (35) and the test cases show that there is also potential for extracting the shape of an arbitrary reflection loss curve from experimental data given adequate signal-to-noise-ratio. Second, it is vital to be able to predict multipath time spreading in order to adjust signal processing integration times. Since the shape of the tail is independent of range it can easily be calculated in advance and incorporated in typical signal processing feature extractors. Third, with perfect knowledge of the environment one might be able to extract a point target by deconvolution of the multipath arrivals. With imperfect knowledge one might have a better chance of deconvolution with the incoherent envelope predicted here since it is less sensitive to the detailed shifts and strengths of the eigenrays while retaining the sharp rise at the leading edge and the correct fall-off. In general this kind of filter (effectively an exponentially weighted smoothing) is invertible.

In addition, analytical and simple numerical approaches imply very short computation times so that these solutions can readily be incorporated in real-time systems, whether aimed at detection and classification or at geoaoustic inversion.

ACKNOWLEDGMENT

The authors would like to thank Alberto Baldacci of NURC for stimulating interest in the refraction version of these pulse shape formulas and some early comparisons with ray traces. Without his enthusiasm this work would not have existed.

APPENDIX A: PULSE SHAPE AS AN EXPLICIT FUNCTION OF TIME

There are two refraction regimes. In the first, rays interact only with the boundary on the c_L side; in the second, they interact with both boundaries. By making approximations the components of pulse shape Eqs. (23) and (35) are written as explicit functions of time.

1. Regime 1 contribution

The expression for t [Eq. (15), main text] is expanded as a series in u then differentiated with respect to t . This series is convergent since the argument of asinh (namely $\tan \theta_L$) is smaller than unity in the region of interest. Therefore one can invert the series (Morse and Feshbach, 1953). Equation (15) is expanded as

$$\begin{aligned} t &= \frac{2ru}{c'} \left(\left(\frac{c'}{2c_L u} \right) - \frac{1}{6} \left(\frac{c'}{2c_L u} \right)^3 + \frac{3}{40} \left(\frac{c'}{2c_L u} \right)^5 \right. \\ &\quad \left. - \frac{5}{112} \left(\frac{c'}{2c_L u} \right)^7 + \dots \right) \\ &= \frac{r}{c_L} \left(1 - \frac{1}{6} \left(\frac{c'}{2c_L u} \right)^2 + \frac{3}{40} \left(\frac{c'}{2c_L u} \right)^4 - \frac{5}{112} \left(\frac{c'}{2c_L u} \right)^6 + \dots \right). \end{aligned} \quad (A1)$$

This can be rearranged as

$$\xi = 1 - tc_L/r = \frac{1}{6}X - \frac{3}{40}X^2 + \frac{5}{112}X^3 - \dots, \quad (A2)$$

$$\text{where } X = \left(\frac{c'}{2c_L u} \right)^2. \quad (A3)$$

The inverse series is

$$X = 6\xi + \frac{81}{5}\xi^2 + \frac{5184}{175}\xi^3 - \dots. \quad (A4)$$

Numerically one can easily evaluate $t(u)$ from Eq. (A1) or (15) and $u(t)$ from Eq. (A4) and plot them on the same graph to demonstrate convergence and consistency. The intensity is given in terms of u by Eq. (2.6) from Harrison (2003b), so following Eq. (1), one needs an expression for du/dt . Differentiating Eq. (A3) with respect to u and Eq. (A2) with respect to t leads to

$$\frac{du}{dt} = \frac{du}{dX} \frac{dX}{d\xi} \frac{d\xi}{dt} = \frac{dX}{d\xi} \left(\frac{2c_L}{c'} \right)^2 \frac{u^3 c_L}{2r} = \frac{dX}{d\xi} \frac{c'}{4rX^{3/2}} \quad (A5)$$

then differentiating Eq. (A4) with respect to ξ and substituting yields

$$\frac{du}{dt} = \frac{1}{4\sqrt{6}r} \frac{c'}{\xi^{3/2}} f(\xi), \quad (A6)$$

where

$$\begin{aligned} f(\xi) &= \frac{\left(1 + \frac{2 \times 81}{6 \times 5} \xi + \frac{3 \times 5184}{6 \times 175} \xi^2 + \dots \right)}{\left(1 + \frac{81}{6 \times 5} \xi + \frac{5184}{6 \times 175} \xi^2 + \dots \right)^{3/2}} \\ &= 1 + \frac{27}{20} \xi - \frac{891}{1120} \xi^2 + \dots \\ &= 1 + 1.35\xi - 0.7955\xi^2 + \dots. \end{aligned} \quad (A7)$$

Because $r/c_L \geq t > r/c_H$, ξ is similarly bounded ($\xi_L \leq \xi < \xi_H$). The limiting values of ξ are $\xi_L=0$, $\xi_H=Hc'/c_H=(c_H-c_L)/c_H$. An extreme case might have $c_H-c_L=30$ m/s so $\xi_H \sim 0.02$. Thus the second term in $f(\xi)$ is very small and the third is quite negligible. Notice that the first-order term in Eq. (A6) (i.e., setting $f=1$) could easily have been obtained directly from Eq. (A1) by taking just the first two terms and differentiating.

The resulting regime 1 contribution to the pulse shape can be written as an explicit function of t (and $t_L=r/c_L$),

$$I_1 dt = \frac{dt}{(t_L - t)^{3/2}} \left\{ \frac{t_L^{3/2} c'}{\sqrt{6} r^2} \exp[-(\alpha_L c' / 2c_L) r] \right\}. \quad (A8)$$

2. Regime 2 contribution

If one expands the asinh terms of Eq. (27)—main text—in a third-order Taylor series about an angle θ_0 intermediate between θ_L and θ_H , where $\tan \theta_0 = 2Hu$, one arrives at

$$t = \frac{r}{2} \sqrt{1 + (2Hu)^2 (A + B/u^2)}, \quad (\text{A9})$$

where

$$A = \left(\frac{1}{c_L} + \frac{1}{c_H} \right) - \frac{(Hc')^2}{12} \left(3 \left(\frac{c_H + c_L}{c_H^2 c_L^2} \right) - \left(\frac{1}{c_L^3} + \frac{1}{c_H^3} \right) \right), \quad (\text{A10})$$

$$B = -\frac{(c')^2}{6 \times 16} \left(\frac{1}{c_L^3} + \frac{1}{c_H^3} \right). \quad (\text{A11})$$

$$\frac{du}{dt} = 1 \left/ \left\{ \frac{t}{u} - \frac{2r}{\sqrt{\{2H(c_H + c_L)\}^2 u^4 + 2(c_L^2 + c_H^2)u^2 + (c'/2)^2}} \right\} \right. \quad (\text{A16})$$

and substituting Eq. (A14) or (A15) in this makes a good approximation which can be used in Eq. (35)—main text—for the pulse shape, but the form is not useful for convolution. A poorer approximation is obtained by differentiating the approximate form, Eq. (A12), to obtain

$$\frac{du}{dt} = \frac{t}{(2Ht_0)^2 u} = \frac{t}{2Ht_0 \sqrt{t^2 - t_0^2}}. \quad (\text{A17})$$

As functions of t these two approximations are, respectively,

$$I_2 dt = \left(\frac{t}{\sqrt{b_1 t + b_0}} - \frac{1}{\sqrt{c_2 t^2 + c_1 t + c_0}} \right)^{-1} \times \exp(-a_1 t - a_0) dt 2Hf_0, \quad (\text{A18})$$

$$I_2 dt = \frac{t}{\sqrt{t^2 - t_0^2}} \exp(-a_1 t - a_0) \frac{1}{t_0} dt f_0, \quad (\text{A19})$$

where the constants $a_0, a_1, b_0, b_1, c_0, c_1, c_2, f_0$ are given by

$$a_0 = r(\alpha_L a_L + \alpha_H a_H) (u_{\min}^2 2t_0 H^2 - t_{\min}) / (t_0 H),$$

$$a_1 = r(\alpha_L a_L + \alpha_H a_H) / (t_0 H),$$

$$b_0 = u_{\min}^2 - \frac{t_{\min}}{2t_0 H^2} \approx \frac{-1}{2H^2},$$

$$b_1 = \frac{1}{2t_0 H^2},$$

Even retaining only the first term of A this is an extremely good approximation. Neglect of B results in a slight discrepancy for early arrivals, but under these conditions the formula can be inverted to give

$$u^2 = ((t/t_0)^2 - 1) / (2H)^2 = \left(\frac{t - t_0}{t_0} \right) \left(\frac{t + t_0}{2t_0} \right) \frac{1}{2H^2}, \quad (\text{A12})$$

where

$$t_0 = \frac{r}{2} \left(\frac{1}{c_L} + \frac{1}{c_H} \right). \quad (\text{A13})$$

This suggests the alternative

$$u^2 = \left(\frac{t - t_{\min}}{t_0} \right) \frac{1}{2H^2} + u_{\min}^2 \quad (\text{A14})$$

or even

$$u^2 = \left(\frac{t - t_{\min}}{t_{\min}} \right) \frac{1}{2H^2} + u_{\min}^2 \quad (\text{A15})$$

Equation (34)—main text—can be written as

$$c_0 = \left(\frac{H}{r} \right)^2 (c_L + c_H)^2 \left(u_{\min}^2 - \frac{t_{\min}}{2t_0 H^2} \right)^2 + \frac{(c_L^2 + c_H^2)}{2r^2} \left(u_{\min}^2 - \frac{t_{\min}}{2t_0 H^2} \right) + \frac{c'^2}{16r^2},$$

$$c_1 = \frac{1}{r^2 t_0 H^2} \left\{ (c_L + c_H)^2 \left(H^2 u_{\min}^2 - \frac{t_{\min}}{2t_0} \right) + \frac{(c_L^2 + c_H^2)}{4} \right\},$$

$$c_2 = \frac{(c_L + c_H)^2}{(2rt_0 H)^2},$$

$$f_0 = \frac{2}{rH} \exp\{-c' r(\alpha_L/c_L - \alpha_H/c_H)/4\}$$

and t_0 is given by Eq. (A13).

APPENDIX B: CAUSTICS, FOCUSING, AND DEPTH AVERAGING

At high frequencies in shallow water it is well known (Brekhovskikh and Lysanov, 1982) that there is a pattern of caustics in depth-range space. The effects of taking a range average of intensity in such a field was investigated by Weston (1980). It is possible to extend his formulas to the two regimes considered here by inserting Wentzel–Kramers–Brillouin (WKB) modes into an incoherent mode sum and then writing modes and wave numbers in terms of a continuum of angles at source, receiver, and seabed (Harrison,

2003b). The relationships among mode normalization, cycle distance, and wave number K come from differentiating the WKB “phase integral” with respect to wave number. The result is

$$\begin{aligned} E &= 2\pi \int \phi_s^2 \phi_r^2 Adn/(Kr) = \int \phi_s^2 \phi_r^2 AdK/(uKr) \\ &= \frac{4}{r} \int \frac{uAdK}{K \tan \theta_s \tan \theta_r} = \frac{4}{r} \int \frac{u \tan \theta_L Ad \theta_L}{\tan \theta_s \tan \theta_r}, \end{aligned} \quad (\text{B1})$$

where $\phi_{s,r}$ are the modes at source and receiver, A is the Gaussian attenuation term already calculated in Secs. III and IV, and the integral limits are understood to span the part of the duct for which angles are real. This is converted to pulse shape by writing

$$Idt = \frac{4}{r} \int \frac{u \tan \theta_L A}{\tan \theta_s \tan \theta_r} \frac{d\theta_L}{dt}. \quad (\text{B2})$$

Comparing this with the regime 1 [Eq. (23), main text] and regime 2 [Eq. (35)] formulas, having used the appropriate relationships between θ_L and u , [Eqs. (13) and (25)] it is found that they differ by “focusing factors” of, respectively,

$$f_1 = \frac{\sin^2 \theta_L}{\tan \theta_s \tan \theta_r}, \quad (\text{B3})$$

$$\begin{aligned} f_2 &= \frac{\sin \theta_L \cos \theta_L}{\tan \theta_s \tan \theta_r} \left(2Hu a_L - \frac{c'}{4c_L u} \right) \\ &\approx \frac{\tan \theta_L \tan \theta_H \cos^2 \theta_L}{\tan \theta_s \tan \theta_r}. \end{aligned} \quad (\text{B4})$$

The first term has the effect of introducing a singularity in intensity whenever the angle at source, or receiver, or both is zero. Both terms tend to $\cos^2 \theta$ for fairly large angles, i.e., the tail of the pulse. It can be shown, by an eigenray derivation, that this is due to the approximation of slant range by horizontal range. Notice that in the application to pulse shape these terms are merely multipliers, so the problems of integration encountered by Weston (1980) are avoided. Inclusion or exclusion of these terms can be regarded as defining a high or low frequency limit.

By making use of the modes’ orthogonality, namely $\int \phi_r^2 dz = 1$, the depth average of Eq. (B1), is simply

$$\begin{aligned} E &= 2\pi \int \phi_s^2 Adn/(KrH) = \int \phi_s^2 AdK/(uKrH) \\ &= \frac{2}{rH} \int \frac{AdK}{K \tan \theta_s} = \frac{2}{rH} \int \frac{\tan \theta_L Ad \theta_L}{\tan \theta_s}. \end{aligned} \quad (\text{B5})$$

In the case of the simplified formulas of Sec. IV the turning point depth h for each ray determines the relevant weighting

h/H in the depth average. For a uniform gradient it can be shown that h is related exactly to u by

$$h = \frac{c_L}{c'} \left(\sqrt{1 + \frac{c'^2}{4u^2 c_L^2}} - 1 \right), \quad (\text{B6})$$

which clearly has the property that it is exactly H when $u = u_{\min}$ [see Eq. (17), main text], it is h_s when $u = u_{\max}$, [Eq. (16)], and it is zero if $\theta_L = 0$ since u would be infinity.

- Ainslie, M. A., and Beerens, S. P. (2005). Sonar equation terms, in “A compendium of definitions for sonar performance measurements and modelling,” edited by M. A. Ainslie, Version 1, TNO Booklet No. AOG-v9, TNO Underwater Technology Dept., The Hague, The Netherlands, pp. 8–23.
- Atkinson, J. E. (1974). “Computer-implemented acoustic channel model,” J. Acoust. Soc. Am. **56**, S1–S18.
- Brekhovskikh, L., and Lysanov, Yu. (1982). *Fundamentals of Ocean Acoustics* (Springer, New York).
- Ferla, C. M., Porter, M. B., and Jensen, F. B. (1993). “C-SNAP: Coupled SACLANTCEN normal mode propagation loss model,” SACLANT Undersea Research Centre, La Spezia, Italy, Memorandum Rep. No. SM-274.
- Hall, M. V. (1995). “Dimensions and units of underwater acoustic parameters,” J. Acoust. Soc. Am. **97**, 3887–3889.
- Harrison, C. H. (2003a). “Closed-form solutions for reverberation and signal-excess with mode-stripping and Lambert’s law,” J. Acoust. Soc. Am. **114**, 2744–2756.
- Harrison, C. H. (2003b). “Signal and reverberation formulae including refraction,” SACLANT Undersea Research Centre, La Spezia, Italy, Rep. No. SR-370 (obtainable through national distribution centers, see <http://www.nurc.nato.int/publications/index.html>). Last viewed 2/7/07.
- Harrison, C. H. (2005a). “Fast bistatic signal-to-reverberation-ratio calculation,” J. Comput. Acoust. **13**, 317–340.
- Harrison, C. H. (2005b). “Closed form bistatic reverberation and target echoes with variable bathymetry and sound speed,” IEEE J. Ocean. Eng. **30**, 660–675.
- Harrison, C. H. (2006). “Multipath pulse shapes with refraction,” NATO Undersea Research Centre, La Spezia, Italy, Rep. No. NURC-FR-2006-005 (obtainable through national distribution centers, see <http://www.nurc.nato.int/pubs/index.html>). Last viewed 2/7/07.
- Morse, P. M., and Feshbach, H. (1953). *Methods of Theoretical Physics* (McGraw-Hill, New York), pp. 411–413.
- Preston, J. R., Ellis, D. D., and Gauss, R. C. (2005). “Geoacoustic parameter extraction using reverberation data from the 2000 Boundary Characterization Experiment on the Malta Plateau,” IEEE J. Ocean. Eng. **30**, 709–732.
- Prior, M., and Harrison, C. H. (2004). “Estimation of seabed reflection properties from direct blast pulse shape,” J. Acoust. Soc. Am. **116**, 1341–1344.
- Sachs, M. B., Sergeant, R. L., and Russotti, J. S. (1968). “Speech intelligibility in a stationary multipath channel,” J. Acoust. Soc. Am. **44**, 385.
- Siderius, M., Nielsen, P. L., and Gerstoft, P. (2002). “Range-dependent seabed characterization by inversion of acoustic data from a towed receiver array,” J. Acoust. Soc. Am. **112**, 1523–1535.
- Smith, P. J. (1971). “The averaged impulse response of a shallow-water channel,” J. Acoust. Soc. Am. **50**, 332–336.
- Urick, R. J. (1967). *Principles of Underwater Sound* (McGraw-Hill, New York).
- Weston, D. E. (1980). “Wave-theory peaks in range-averaged channels of uniform sound velocity,” J. Acoust. Soc. Am. **68**, 282–286.

Document Data Sheet

<i>Security Classification</i>		<i>Project No.</i>
<i>Document Serial No.</i> NURC-PR-2007-002	<i>Date of Issue</i> April 2007	<i>Total Pages</i> pp. 15
<i>Author(s)</i> Chris H. Harrison, Peter L. Nielsen		
<i>Title</i> Multipath pulse shapes in shallow water: Theory and simulation		
<i>Abstract</i> .		
<i>Keywords</i>		
<i>Issuing Organization</i> NURC Viale San Bartolomeo 400, 19126 La Spezia, Italy [From N. America: NURC (New York) APO AE 09613-5000]		Tel: +39 0187 527 361 Fax: +39 0187 527 700 E-mail: library@nurc.nato.int